PERGAMON

International Journal of Multiphase Flow 26 (2000) 1037–1061

International Journal of Multiphase Flow

www.elsevier.com/locate/ijmulflow

Flow patterns in small diameter vertical non-circular channels

G. Wölk*, M. Dreyer, H.J. Rath

Center of Applied Space Technology and Microgravity, University of Bremen, 28359, Bremen, Germany

Received 31 March 1998; received in revised form 11 June 1999

Abstract

Experiments have been performed for upwards vertical two-phase air–water flow through one circular and four different non-circular channels (with rectangular, rhombic and equilateral triangular cross-section) with an equivalent (hydraulic) diameter of $d_h \approx 6$ mm. Three of the four basic flow patterns were observed depending on the liquid and gas superficial velocity. The transition from dispersed bubble to slug flow, from dispersed bubble to churn flow and from slug to churn flow is being discussed. Based on existing models, theoretical approaches for the prediction of flow pattern transitions are qualified to achieve more satisfactory results for capillary tubes/channels. New distribution parameters for the rhombic and equilateral triangular channel are determined. For the transition from slug to churn flow, the flooding model is improved to predict the transition for non-circular channels as well as for circular tubes. A value for the unknown constant C for the flooding model providing good results is suggested. The transition from dispersed bubble to slug flow is modeled in consideration of the superficial liquid and gas velocity and in consideration of the hydraulic diameter. Good agreement between theory and experiment is obtained.

Keywords: Vertical gas–liquid flow; Non-circular channels; Flow pattern; Drift-flux model; Flooding model

1. Introduction

Gas/liquid two-phase flow is of great importance in a wide range of technical applications, e.g. in heat transfer systems, distillation processes and steam generators. In comparison with single-phase flow systems one may achieve the same efficiency factor with reduced flow rates.

* Corresponding author.

0301-9322/00/$ - see front matter
PII: S0301-9322(99)00069-5

For the optimization of the design and the operation of two-phase flow systems, especially concerning the pressure drop and the thermodynamical quantities (e.g. the heat transfer coefficient), there is a need for the engineer to predict accurately the existing flow patterns (e.g. Bell, 1988). Designing a compact heat transfer system one may utilize the enthalpy of vaporization during the phase transition of the liquid. Knowledge of the flow patterns is necessary to apply an appropriate fluid-dynamic or heat transfer theory.

Designing a heat transfer system, one has to take into consideration different possible geometries. On earth, double-pipe heat exchanger and tubular heat exchanger are in use predominately. However, non-circular channels/ducts are suited very well for heat transfer applications such as plain-fin compact heat exchangers, because the ratio between circumference and cross-section area is more advantageous as for circular tubes and this allows to increase the heat transfer rates. Furthermore, considering the single-phase flow in non-circular channels a so-called turbulent secondary flow occurs (Nikuradse, 1933), which also increases the heat and mass transfer. One might expect that these turbulent secondary flows have also considerable influence on the two-phase flow in non-circular channels.

The present paper studies the upwards vertical two-phase flow in one circular and four different non-circular channels with an equivalent (hydraulic) diameter of $d_h \approx 6$ mm. The equivalent diameter lies in the typically range used for plate-fin heat exchangers (1–10 mm). The experimental results are illustrated and different flow pattern models for vertical upwards two-phase flow were verified against the data. Improvements of these models are suggested in order to take into account the cross-section geometry of the non-circular channels.

1.1. Flow patterns in vertical two-phase flow

In case of vertical upwards two-phase flow four main flow patterns, designated by Hewitt and Hall-Taylor (1970) as bubble flow, slug flow, churn flow and annular flow, can be observed. The characteristics of these basic flow patterns are described as follows:

1. Bubble flow: The gas is dispersed forming discrete bubbles in the continuous liquid. The bubbles may have different shapes and sizes but they are smaller than the pipe diameter. In vertical upwards two-phase flow the bubble flow is subdivided into a non-dispersed and a dispersed bubble flow.
2. Slug flow: When the bubble concentration in bubble flow increases, bubble coalescence occurs and forms larger bubbles of a size similar to the pipe diameter. These so called Taylor bubbles have a characteristic spherical cap nose and are somewhat abruptly terminated. The bubbles are separated by liquid slugs containing smaller bubbles in it. The Taylor bubbles move upwards and are separated from the wall by a thin liquid film that flows vertically downwards.
3. Churn flow: Churn flow is a highly disordered, chaotic and frothy flow regime with a typical oscillatory motion of the liquid. In churn flow the gas bubbles become narrow and more irregular compared to slug flow and the continuity of the liquid between the gas bubbles is repeatedly destroyed by a high local gas concentration in the liquid.
4. Annular flow: The characteristic of annular flow is the continuity of the gas phase in the

center of the tube. The liquid phase flows upwards partially as a film along the walls of the tube, and partially as droplets in the central gas core.

The transition between two different flow regimes is a gradual phenomenon and no definite transition point exists. Consequently, it is possible to observe some transition flow patterns with the characteristics of two of the flow pattern types described above.

1.2. Flow pattern maps

For an engineer in designing a two-phase flow system, it is important to predict accurately the existing flow patterns for given phase properties, flow rates and for a given channel geometry. For that one can normally obtain the flow pattern transitions from flow pattern maps. In the last decades different types of flow pattern maps have been developed empirically after evaluation of experiments or theoretically. One of the first was given by Duns and Ros (1963), however newer models were presented for example by Taitel et al. (1980), Weisman and Kang (1981), Barnea et al. (1982), Mishima and Ishii (1984) and McQuillan and Whalley (1985) for an overall flow pattern map or by Jayanti and Hewitt (1992) only for the transition from slug to churn flow. Most of the models show agreement in comparing them directly with experimental results for the flow pattern transition in circular tubes having a diameter above 20 mm. However, the comparison of experimental results for small diameter tubes or narrow channels with the developed models shows poor agreement, (e.g. Lowry and Kawaji, 1988; Fukano and Kariyasaki, 1993). Only the theoretical model from Mishima and Ishii (1984) is developed to predict the transition in small diameter circular tubes or rectangular channels for an overall flow pattern map and the comparison with air–water data shows some reasonable agreement (e.g. Wilmarth and Ishii, 1994), however Mishima and Ishii (1984) made no distinction between non-dispersed and dispersed bubble flow. Other than that mentioned there only exist two transition models for predicting the transition to annular flow in small diameter tubes from Barnea et al. (1983) and Jones and Zuber (1979).

2. Experimental methods

2.1. Experimental setup

The experiment facility used for the present study was developed for microgravity experiments in the drop tower of Bremen as well as for normal gravity experiments. The apparatus consists of a closed liquid flow loop subdivided into two parallel test sections, two gas flow loops, two mixing systems, two pump units, a separator unit, an electronic unit and a data acquisition system. A schematic representation of one of the two air–water loops is shown in Fig. 1.

The working fluids are air and deionized water with minutes amounts of salt dissolved in it for measuring the void fraction. Water can be pumped in a closed flow loop from the water reservoir to the test sections and back to the separator unit. The separator unit again is in direct contact with the water reservoir. The water flow rate is adjusted and measured separately

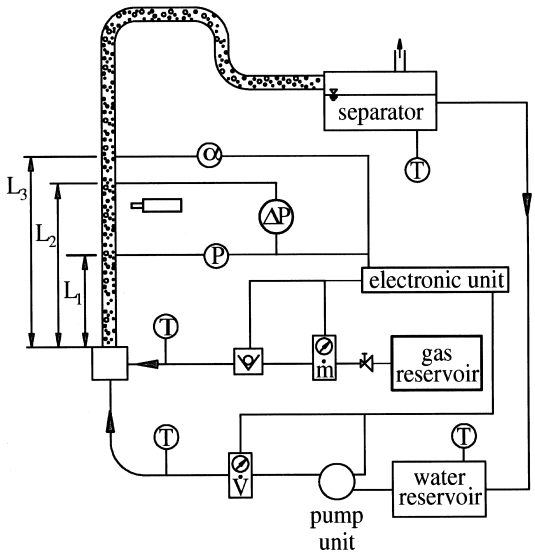

Fig. 1. Schematic representation of the experimental system for one of the two test sections.

for each test section with a volume flow rate controller (model RCQ02, Rösler and Cie. Instruments GmbH) and the water flows axially in the mixing sections. Air is stored in a 10 l tank under an initial pressure of 8 bar which will be reduced by a pressure valve to a value of 3 bar. The air is cleaned with a super fine filter and has a cleanliness of 99.999% (model LFM-1/8-S, Festo Pneumatic). The gas flow rate is also adjusted and measured separately with a volume flow rate controller (model F-201C-FB-22-V Bronkhorst Hi-Tech B.V.) for each test section and it is discharged into the water flow through a small filter element with an average pore size distribution of 150 μm in the mixing systems. The air–water mixing system is illustrated in Fig. 2. The direction of the filter element is perpendicular to the flow direction of the fluid and the thread reach can be modified. The maximum thread reach extends to the central axis of the mixing system (with $t_e = 0$ mm). This is the 'normal' arrangement for the experiments. For one cross-section geometry the thread reach was narrowed about $t_e = 2$ mm from the central axis. In the following discussion, we described this experimental condition as mixing technique MT2. The gas flow rate controller is calibrated for an initial pressure value of

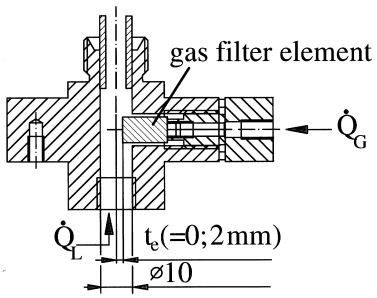

Fig. 2. Air–water mixing system with two different thread reaches for the gas filter element.

3 bar and a temperature of 20°C. The homogenous mixture of air and water then flows into the test sections manufactured from transparent PMMA. Each test section has a length of 920 mm and above each section exists an outlet region with a length of 400 mm. For each test section there are five geometries which are depicted in Fig. 3. As an equivalent diameter for the comparison of the results serves the hydraulic diameter defined as (White, 1986):

$$d_h = 4\frac{A}{\Gamma}, \tag{1}$$

where A is the total cross-section area and Γ is the wetted perimeter of the cross-section. For the test section of our study the hydraulic diameter is $d_h \approx 6.0$ mm. The dimensions of the channels are presented in Table 1, where d_h is the hydraulic diameter, s is the gap and w is the width of the rectangular flow channels, b is the width and h is the height of the rhombic flow channel, a is the length of the equilateral triangular flow channel, respectively. The angle of spread of the rhombic test section is $2\varphi = 60^\circ$.

The absolute pressure is measured at a distance of $L_1 = 465$ mm behind the mixing unit and the pressure drop across a length of 250 mm in the test section can be measured by a differential pressure transducer (wet/wet). In between that length the visual section is placed at a distance of $L_2 = 580$ mm behind the mixer. The air/water flow is recorded by a video camera using a shutter speed of 1/2000 s. The void fraction can be obtained from conductive probes placed upstream from the visual section before the outlet of the test section at a distance of $L_3 = 800$ mm behind the mixer. After passing the test sections, the air/water mixture flows into a separator unit, from which the gas escapes to the ambient and the water returns to the water reservoir. Depending on the cross-section of the channel-geometry, the superficial velocities of the liquid and the gas (at atmospheric pressure) are in the range of 0.36 to 4.0 and 0.15 to 5.0 m/s, respectively.

2.2. Experimental uncertainties

The quantities of the direct measurements are the flow rates, the absolute pressure and the pressure drop. The air flow rate was measured with an accuracy of ± 0.4 and the water flow

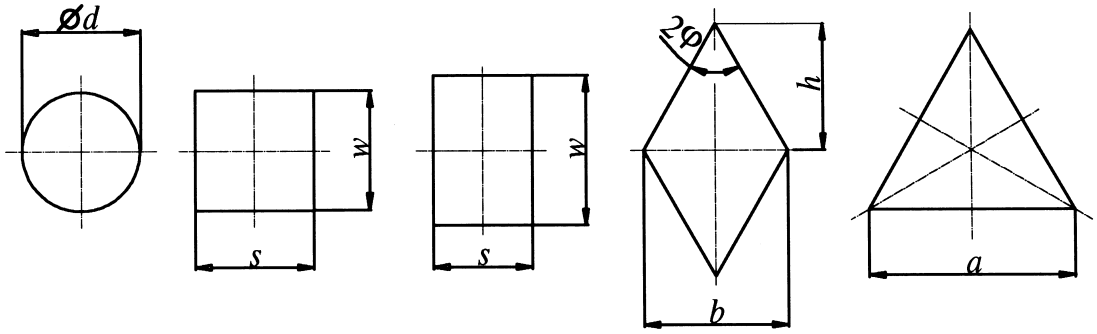

Fig. 3. Cross section geometries of the five test sections.

rate with an accuracy of ±1.0%, the absolute pressure with an accuracy of ±0.7% and the pressure drop with an accuracy of ±5.0%. The channel dimensions were estimated with an microscope and/or with a calliper gauge and the accuracy was better than 1%. The accuracy of the other quantities, such as lengths and properties, was estimated as 0.15% and 0.25%, respectively.

2.3. Experiment results

The flow patterns were discerned based on visual observation of a video tape replay (25 frames/s). Three different flow patterns were identified and named as dispersed bubble flow, slug flow and churn flow following the flow pattern definition in Section 1.1. Annular flow was not observed due to the superficial gas velocity boundary range (5 m/s) and non-dispersed bubble flow was not identified corresponding to Taitel et al. (1980). They presented a relation for calculating the minimum tube diameter for the existence of non-dispersed bubble flow. Below this minimum hydraulic diameter (for air–water two-phase flow: $d_h \approx 5.1$ cm) the non-dispersed bubble flow will not exist. In accordance with the definition from Hewitt and Hall-Taylor (1970) and in contrast to Mishima and Ishii (1984) and Jayanti and Hewitt (1992), the latter referring to the experimental results from Owen (1986), we could not identify slug flow at high liquid flow rates. If the liquid flow rate is high ($U_{LS} > 1.0$–1.5 m/s depending on the cross-section geometry), there is a high local gas concentration in the liquid flow with many small irregular gas bubbles in the liquid. With increasing gas flow rate for a constant liquid flow rate the transition occurs directly from dispersed bubble to churn flow, whereas in this churn flow domain liquid regions without many small gas bubbles do not exist. Beside gas bubbles having a diameter much greater than the tube diameter there also exist a very high gas concentration of small gas bubbles in the liquid.

The flow pattern maps are displayed in Figs. 4–8 for the circular tube, two rectangular channels ($s/w = 0.97$ and $s/w = 0.7$), the rhombic channel and for the equilateral triangular channel, respectively. For the axis of the figures, we use the superficial gas velocity U_{GS} and the superficial liquid velocity U_{LS}. Solid symbols denote transition flow patterns with the characteristic of two basic flow patterns. Since the error bars are smaller than the symbols in the figures, we do not present the error bars in the figures. The curves in the figures display the transition criteria which will be discussed in detail in Section 3. From Figs. 4–8, it can be observed that for small channel diameter the cross-section geometry directly influences the

Table 1
Dimensions of the five geometries

Geometry	d_h (mm)	Lengths (mm)	
Circular	5.9		
Rectangular ($s/w = 0.97$)	6.1	$s = 6.0$	$w = 6.2$
Rectangular ($s/w = 0.7$)	5.9	$s = 5.0$	$w = 7.2$
Rhombic ($\varphi = 30°$)	6.3	$b = 7.27$	$h = 6.3$
Equilateral triangula r	6.1	$a = 10.43$	

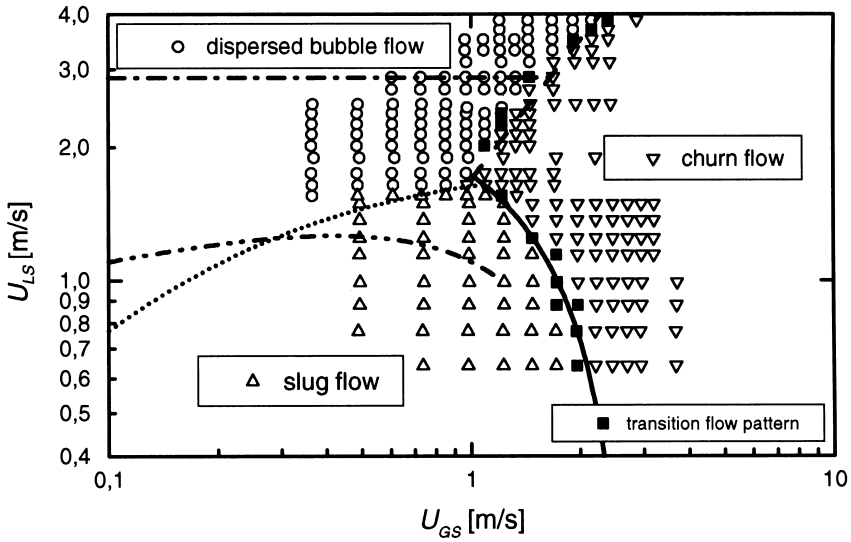

Fig. 4. Flow pattern map for a vertical upwards air–water two-phase flow in a circular tube with $d_h = 5.9$ mm, 23°C and the transition criteria: (- - -) Eq. (2), (———) Eq. (9) with $C = 1.21$, (.....) Eq. (22) with $U_{LS}/\phi_{2,new}$, – · – Weisman and Kang (1981) and (-..-), Barnea et al. (1982).

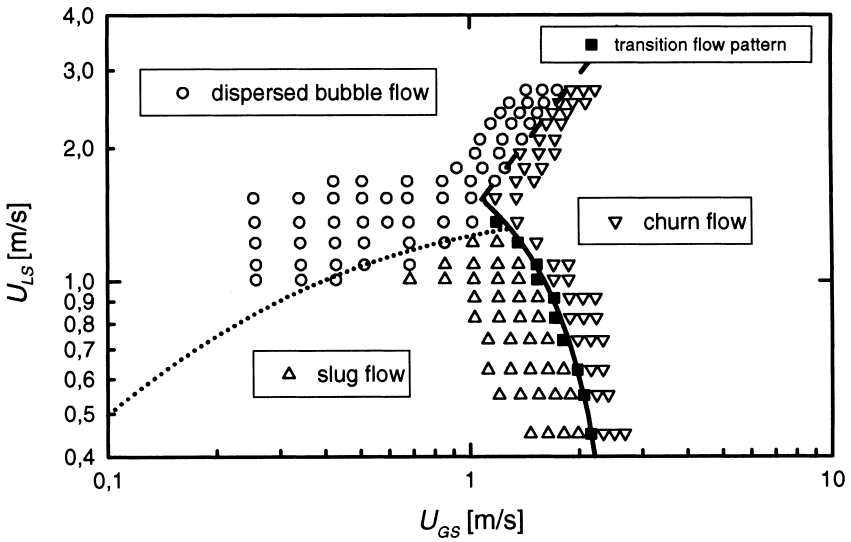

Fig. 5. Flow pattern map for a vertical upwards air–water two-phase flow in a rectangular channel ($s/w = 0.97$) with $d_h = 6.1$ mm, 22°C and the transition criteria: (- - -) Eq. (2), (———) Eq. (9) with $C = 1.18$ and (.....) Eq. (22) with $U_{LS}/\phi_{2,non\text{-}circular}$.

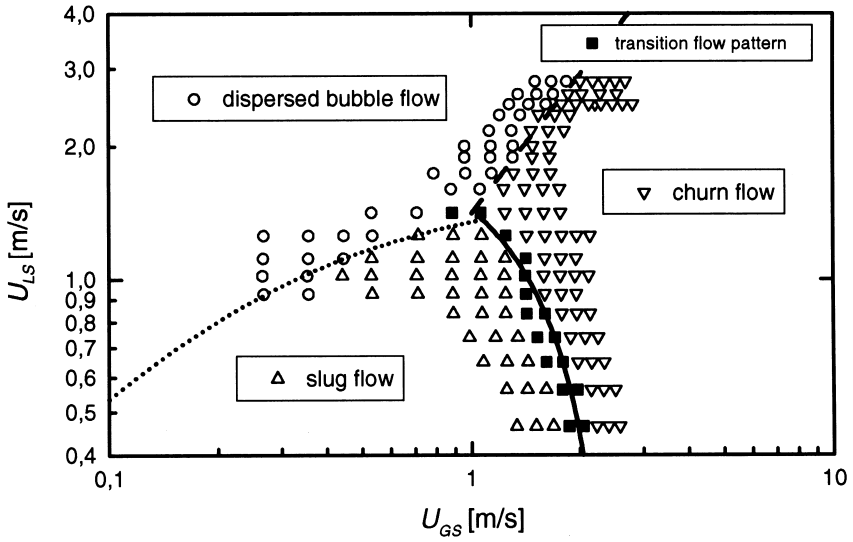

Fig. 6. Flow pattern map for a vertical upwards air–water two-phase flow in a rectangular channel ($s/w = 0.70$) with $d_h = 5.9$ mm, 22°C and the transition criteria: (- - -) Eq. (2), (———) Eq. (9) with $C = 1.17$ and (.....) Eq. (22) with $U_{LS}/\phi_{2,non\text{-}circular}$.

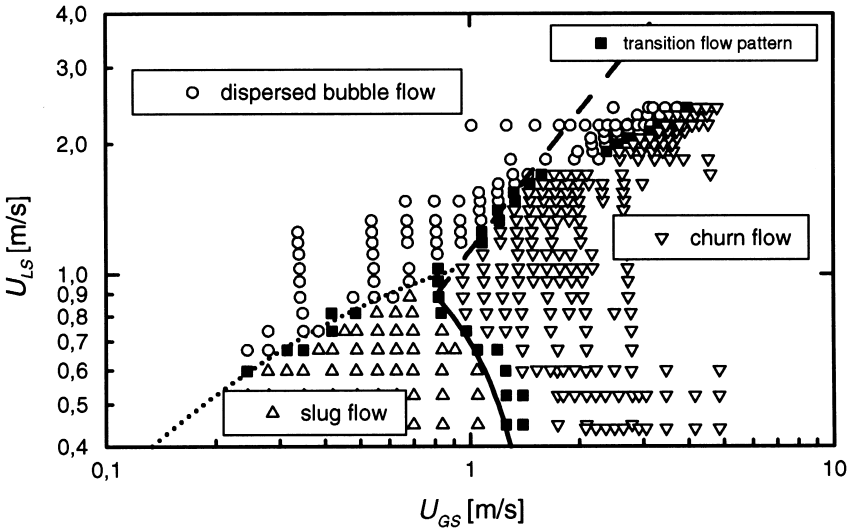

Fig. 7. Flow pattern map for a vertical upwards air–water two-phase flow in a rhombic channel with $d_h = 6.3$ mm, 21°C and the transition criteria: (- - -) Eq. (2), (———)Eq. (9) with $C = 1.19$, and (.....) Eq. (22) with $U_{LS}/\phi_{2,non\text{-}circular}$.

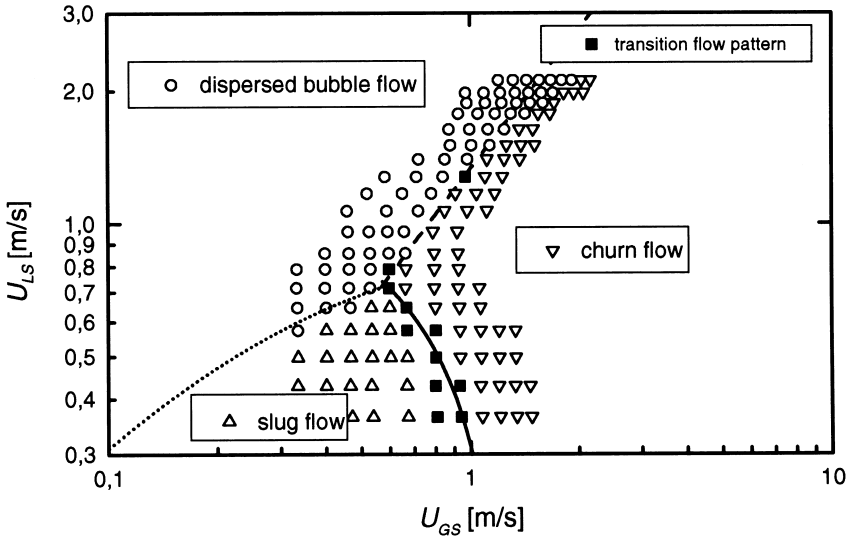

Fig. 8. Flow pattern map for a vertical upwards air–water two-phase flow in an equilateral triangular channel with $d_h = 6.1$ mm, 22°C and the transition criteria: (- - -) Eq. (2), (———) Eq. (9) with $C = 1.20$ and (.....) Eq. (22) $U_{LS}/\phi_{2,\text{non-circular}}$.

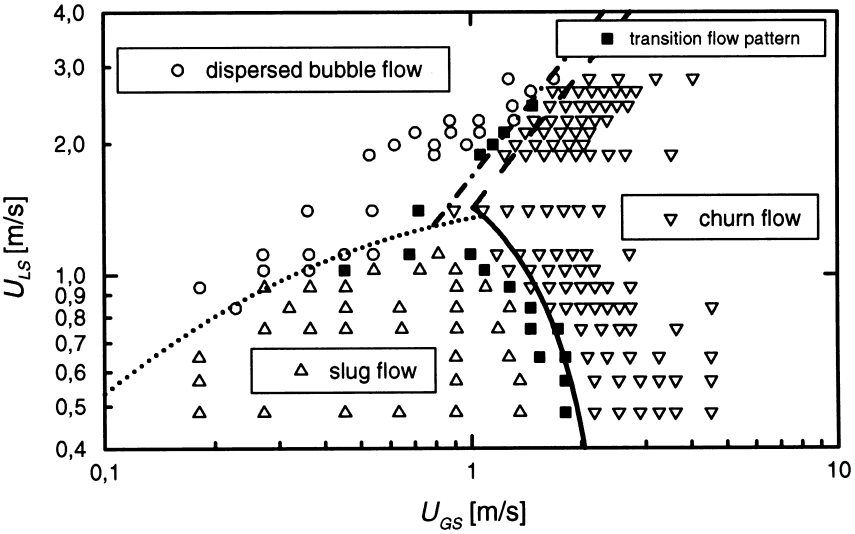

Fig. 9. Flow pattern map for a vertical upwards air–water two-phase flow in a rectangular channel ($s/w = 0.7$) for the mixing technique MT2 with $d_h = 5.9$ mm, 22°C and the transition criteria: (– · –) Eq. (2) with $\alpha = 0.27$, (- - -) Eq. (2) with $\alpha = 0.30$, (———) Eq. (9) with $C = 1.17$ and (.....) Eq. (22) with $U_{LS}/\phi_{2,\text{non-circular}}$.

transition between different flow patterns in contrast to the results reported by Sadatomi et al. (1982) for tube/channel diameters above 10 mm.

The second flow pattern map for the rectangular channel ($s/w = 0.7$) using mixing technique MT2 is shown in Fig. 9. One of the curves (the $- \cdot -$ curve) display the transition criterion from dispersed bubble to churn flow of the MT2 arrangement for the rectangular channel (described in Section 3) and the other three curves display the transition criteria of the 'normal' arrangement for the rectangular channel (also described in Section 3). As might be expected the direct comparison of Figs. 6 and 9 shows that the transition region from dispersed bubble to churn flow and the transition region from slug to churn flow is shifted for the 'normal' arrangement to higher gas flow rates compared to the MT2 arrangement. The phases are mixed at the flow inlet and the resulting flow pattern will depend on how the phases are mixed. If the maximum thread reach of the filter element is extended (the 'normal' arrangement) most of the filter element is located directly within the sphere of influence of the fluid flux and the gas is dispersed as small bubbles. For the MT2 arrangement the sphere of influence of the fluid flux on the filter element is reduced and this mixing technique allows the gas to enter the tube as 'bigger bubbles'. Thus, for the field of lower liquid flow rates churn flow was observed at lower gas flow rates. Only for very high liquid flow rates the mixing technique could be neglected due to the high turbulent motion within the volume flux. The energy in the liquid flux is high enough to break large bubbles into smaller ones. This results is in consistence to the paper published by Liu (1993). He showed for high liquid flow rate condition that there are no significiant differences in the development of the void fraction and bubble size along the length of the flow channel behind a L/d_h-ratio of 60. However, for low liquid flow rate condition the phase development depends on the bubble size and thus on the bubble generation at the inlet.

3. Discussion of the flow pattern transition

In this section the transition from dispersed bubble to slug flow, from dispersed bubble to churn flow and from slug to churn flow is being discussed. At first, we compare useful existing theoretical models with the experimental results (discussed in Section 2.3) and then, if necessary, we improve these models to predict accurately the transition between two different flow patterns for the circular tube and for the four different non-circular channels. The particular interest of this paper consists of the behavior of two-phase flow in small diameter channels/tubes with different geometries, which lies in the typically range used for plate-fin heat exchangers, and in the comparison of the results for the flow pattern transition for the five different cross-section. The comparison of the geometries could give a better understanding of the channel geometry influence and thus of the turbulent secondary flow influence on the flow pattern transition.

3.1. The transition from dispersed bubble to churn flow

The transition from dispersed bubble to churn flow occurs as well as the transition from non-dispersed bubble to slug flow mainly due to agglomeration and coalescence of smaller

bubbles to form larger ones. Additionally, a second criterion for the transition from dispersed bubble flow consists in the bubble breakup caused by turbulent fluctuation in the tube. The turbulent breakup forces tend to break larger bubbles and disperse them uniformly within the tube.

Mishima and Ishii (1984), Mishima et al. (1993) and Mishima and Hibiki (1996) show that the drift-flux model gives a good prediction for the transition from dispersed bubble flow for small diameter circular tubes as well as for small rectangular channels. We will refer to these papers though they make no distinction between non-dispersed and dispersed bubble flow. The drift-flux model is defined as (e.g. Wallis, 1969):

$$u_G = \frac{U_{GS}}{\alpha} = C_0(U_{GS} + U_{LS}) + V_{GU}, \tag{2}$$

where u_G is the gas velocity, α is the channel average void fraction, C_0 is the distribution parameter and V_{GU} is the drift velocity, respectively. The drift velocity for bubble flow is defined as (Mishima and Ishii, 1984):

$$V_{GU} = (1-\alpha)^{7/4}\sqrt{2}\left(\frac{\sigma g \Delta\rho}{\rho_L^2}\right)^{1/4} \tag{3}$$

where ρ_G is the gas density, ρ_L is the liquid density, $\Delta\rho(=\rho_L - \rho_G)$ is the difference of the densities of the two phases, σ is the surface tension of the liquid and g is the terrestrial gravity, respectively. The distribution parameters C_0 for dispersed bubble flow in circular and rectangular channels proposed by Mishima and Ishii (1984) are listed in Table 2. The most important parameter for these transition model is the void fraction.

Radovcich and Moises (1962) provided a semi-theoretical approach postulating that the transition takes place when the frequency of collisions of the discrete bubbles is very high. It was shown that this happens at a void fraction of $\alpha = 0.30$. Mishima and Ishii (1984) made a geometrical consideration that bubble flow would become unstable also at a void fraction value of $\alpha = 0.30$. The experiments for the rectangular channel ($s/w = 0.7$, displayed in Figs. 6 and 9) with the two different mixing systems show that using the drift-flux model to predict the transition, the void fraction for the transition could be shifted from $\alpha \approx 0.27$ for MT2 to $\alpha = 0.30$ for the 'normal' arrangement of the mixing system. To clarify this phenomenon both criteria (the $-\cdot-$ curve with Eq. (2) and $\alpha = 0.27$ and the - - - curve with Eq. (2) and $\alpha = 0.30$) for the transition from dispersed bubble to churn flow are displayed in Fig. 9. This comparison reflects the inconsistence in the literature (e.g. Liu, 1993) between different transition void

Table 2
Distribution parameter C_0 for dispersed bubble flow distributed by Mishima and Ishii (1984) for the circular and rectangular cross-section and determined from the experiments for the rhombic and equilateral triangular cross-section

	Circular	Rectangular	Rhombic	Equilateral triangular
C_0	$1.2 - 0.2\sqrt{\frac{\rho_G}{\rho_L}}$	$1.35 - 0.35\sqrt{\frac{\rho_G}{\rho_L}}$	$1.50 - 0.35\sqrt{\frac{\rho_G}{\rho_L}}$	$1.39 - 0.35\sqrt{\frac{\rho_G}{\rho_L}}$

fraction values. Thus, in consideration of the theoretical approaches and the experiments in the following, we use for the transition from dispersed bubble to churn flow the theoretical void fraction value of 0.30. In Figs. 4–6, it is clearly seen that the drift-flux model gives a good prediction for the transition from dispersed bubble to churn flow for the small circular tube as well as for the rectangular channels under consideration of the theoretical transition void fraction value.

Not known a priori is the distribution parameter for the rhombic and the equilateral triangular channel. Since C_0 represents beside the distribution of the gas phase inside the liquid in the tube/channel also the slope of the transition curve for a constant void fraction value, we estimated the distribution parameter for both channel geometries with fitting the slope of the transition curve under the assumption of a constant transition void fraction value $\alpha = 0.30$ and of the drift velocity mentioned in Eq. (3). As a result of this fit, we get a similar expression as Mishima and Ishii (1984) used for the rectangular channels to predict C_0 for the rhombic and equilateral triangular channel. The determined values are listed in Table 2 and the distribution parameters were estimated with an uncertainty of ± 0.6. For the non-circular channels in comparison to the circular tube the larger C_0 means that the radial distribution of the phases and/or velocity is steeper, the shape of the distribution might be different from that in a circular tube. The transition for the rhombic and equilateral triangular channel is shown in Figs. 7 and 8.

For the rhombic and the equilateral triangular test section a shift of the transition region from $\alpha = 0.30$ to higher values for the void fraction is discerned at superficial liquid velocity of $U_{\mathrm{LS}} > 1.8$ and $U_{\mathrm{LS}} > 1.6$ m/s, respectively. We assume that due to the sharp edges of the respective cross-sections the influence of the turbulent secondary flow is increased intensifying the turbulent motion and thus the kinetic energy in the turbulent volume flow and this causes as an additional shear force on the dispersed bubbles preventing the agglomeration of the gas bubbles. The result is a shift of the transition void fraction value from $\alpha = 0.30$ to higher values. Nearly the same behavior can be observed for the rectangular cross-section ($s/w = 0.7$) using MT2 (shown in Fig. 9). The transition void fraction lies for $U_{LS} = 1.4$–2.6 m/s in the range of $\alpha \approx 0.27$. However, for higher superficial liquid velocities the void fraction value may also be increased to higher α values. Further experiments shall examine, if some kind of shift also exist for higher liquid flow rates for the other geometries. Referring to the papers from Barnea et al. (1982) or McQuillan and Whalley (1985), which focused on larger circular tubes, the transition from dispersed bubble to churn flow is shifted to a void fraction value of $\alpha = 0.52$ or $\alpha = 0.74$. The open question is, whether there exists a dependency between the turbulent kinetic energy and the void fraction value for the transition.

3.2. The slug to churn flow transition

An overview about different slug to churn flow transition mechanism is given by Jayanti and Hewitt (1992). They show for two-phase flow in circular tubes that the flooding model of McQuillan and Whalley (1985) gives satisfactory results at low and high liquid flow rates, respectively. For an explanation of flooding see Wallis (1969). As a basis equation for the flooding mechanism the semi-empirical equation proposed by Wallis (1961) and Hewitt and Wallis (1963) is used:

$$\sqrt{U^*_{GS}} + \sqrt{U^*_{LS}} = C, \tag{4}$$

where C is a constant near to unity and U^*_{GS} and U^*_{LS} are dimensionless gas and liquid superficial velocities, respectively. For the flooding case these dimensionless velocities are defined as:

$$U^*_{GS} = U_{GS}\sqrt{\frac{\rho_G}{g d_h \Delta\rho}} \quad \text{and} \quad U^*_{LS} = U_{LS}\sqrt{\frac{\rho_L}{g d_h \Delta\rho}}. \tag{5}$$

The link between flooding and the slug to churn flow transition is established by McQuillan and Whalley (1985) using the superficial Taylor bubble velocity (U_{BS}) as the characteristic superficial gas velocity and the superficial liquid falling film velocity (U_{FS}) as the characteristic superficial liquid velocity in Eq. (5). Fig. 10 shows the model of slug flow of McQuillan and Whalley (1985). The definition for the superficial Taylor bubble velocity is given by Nicklin et al. (1962) and can be written as a drift-flux model equation (e.g. Eq. (2)):

$$U_{BS} = \alpha\big[C_0(U_{GS} + U_{LS}) + V_{GU}\big]. \tag{6}$$

Here, the distribution parameter C_0 is the same as the one for dispersed bubble flow shown in Table 2 and the drift velocity V_{GU} for the slug flow region is listed in Table 3. The void fraction results from a simple geometric analysis:

$$\alpha = \frac{A_G}{A} = \frac{(d_h - 2\delta)^2}{d_h^2} = \frac{d_h^2 - 4\delta d_h + 4\delta^2}{d_h^2} \approx \left(1 - 4\frac{\delta}{d_h}\right), \tag{7}$$

where A_G is the average cross-section occupied by the gas phase and δ is liquid film thickness in the Taylor bubble region whereas δ is calculated according to a correlation from Brotz (1954) (see Jayanti and Hewitt, 1992). The second order term of the film thickness is neglected. Finally, McQuillan and Whalley are using a continuity equation to calculate the liquid falling film velocity (U_{FS}):

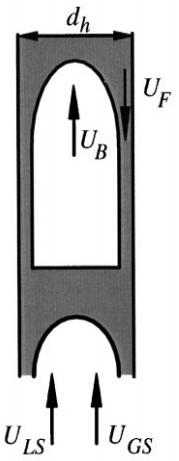

Fig. 10. The model of slug flow from McQuillan and Whalley (1985).

$$U_{FS} = U_{BS} - (U_{GS} + U_{LS}). \tag{8}$$

As an improvement according to the model published by McQuillan and Whalley (1985), Jayanti and Hewitt (1992) are showing that there exist an influence of the channel length L on flooding and they enhance Eq. (4) by a coefficient m which is a function of L/d_h. As a conclusion Jayanti and Hewitt predict the following equation to calculate the transition from slug to churn flow in a circular tube (in consideration of Eqs. (5)–(8):

$$\sqrt{U^*_{GS}} + m\sqrt{U^*_{LS}} \geq C. \tag{9}$$

The remaining unknown is the constant C which depends to some extent on other parameters such as inlet/outlet conditions and the tube length. Fig. 4 shows the correspondence between the flooding model and the experimental results for the circular tube with $C = 1.21$.

From the paper published by Jayanti and Hewitt (1992) and from the discussion above one could see that the rectified flooding model (Eq. (9)) yields good results for predicting the transition from slug to churn flow in circular tubes. For vertical upwards two-phase flow in non-circular channels only one model is available to predict the transition from slug to churn flow (Mishima and Ishii, 1984). This model was also discussed by Jayanti and Hewitt (1992) (for circular tubes) and they show that the agreement of this model to predict the transition from slug to churn flow is probably fortuitous. Since no correlation using the flooding model exists for the slug to churn flow transition in non-circular channels as examined in the present study we improved the rectified flooding model (Eq. (9)) to work also for non-circular channels. The problem to be solved is to determine the void fraction for the Taylor bubble in the region (see definition in Eq. (7)) where the transition occurs. Since the geometry of a circular tube differs to the geometry of a non-circular channel the flooding model as discussed above is not adaptable. Therefore, an analysis to approximate α is presented here for the non-circular channels. The problem for the non-circular channels is to determine the cross-sectional shape of the Taylor bubble, and thus to calculate the average cross-section occupied by the gas. The following geometrical analysis is carried out exemplarily for the rectangular cross-section to evaluate the void fraction used in Eqs. (6) and (7). The total cross-section area for the rectangular channel is:

$$A = sw. \tag{10}$$

For the determination of the gas section area it is assumed that

Table 3
Drift velocity V_{GU} for slug flow and approximated values of the void fraction α for the Taylor bubble region

Geometry	VGU	α
Circular	$0.35\sqrt{(\frac{\Delta\rho g d_h}{\rho_L})}$	$1 - \delta\frac{4}{d_h}$
Rectangular	$(0.23 + 0.13\frac{s}{w})\sqrt{\Delta\rho g w \rho_L}$	$\frac{1}{2}(1 + \frac{\pi}{4}) - \delta(\frac{s+w}{sw})(1 + \frac{\pi}{4})$
Rhombic	$(0.23 + 0.13\frac{s_1}{w_1})\sqrt{\frac{\Delta\rho g w_1}{\rho_L}}$	$\frac{1}{2}(1 + \frac{\pi}{4}) - \delta(\frac{1}{b}\frac{4+\pi}{\cos(\varphi)})$
Equilateral triangula r	$0.35\sqrt{(\frac{\Delta\rho g d_h}{\rho_L})}$	$\frac{1}{2}(1 + \frac{\pi}{3\sqrt{3}}) - \delta(\frac{1}{a}\frac{5\sqrt{3-8}}{3})$

- the fluid film thickness between the wall and the Taylor bubble in the central axis of each channel wall is small compared to the length of the channel wall,
- the fluid film thickness between the wall and the Taylor bubble in the central axis of each channel wall can be calculated with the empirical correlation from Brotz (1954) regardless of the real shape of the Taylor bubble and regardless that the cross-section deviates from a circular tube,
- the fluid film thickness between the wall and the Taylor bubble in the central axis of each channel wall is equal for each side of the rectangular channel ($\delta_1 \approx \delta_2 \approx \delta$).

At first, we consider the maximum cross-section the gas would occupy if the fluid film thickness is constant along each wall and equal to the value in the central axis:

$$A_{G1} = (s - 2\delta)(w - 2\delta) = sw - 2(s + w) + 4\delta^2. \tag{11}$$

This is a non-realistic consideration. Due to the surface tension force acting on the interface between the liquid and the gas, the curvature of the Taylor bubble is rounded and the bubble is not forced into the corner as illustrated in Fig. 11a. In contrast we determine a round cross-section with an elliptical shape as shown in Fig. 11b:

$$A_{G2} = \pi\left(\frac{s}{2} - \delta\right)\left(\frac{w}{2} - \delta\right) = \pi\frac{sw}{4} - \delta\frac{\pi}{2}(s + w) + \pi\delta^2. \tag{12}$$

For this case the cross-section of the gas bubble is to small in contrast to A_{G1} which would be to large, and thus we use the average value between the two cross-sections described above (Eqs. (11) and (12)):

$$A_G \approx \frac{A_{G1} + A_{G2}}{2} = \frac{sw\left(1 + \frac{\pi}{4}\right) - \delta(s + w)\left(2 + \frac{\pi}{2}\right) + (4 + \pi)\delta^2}{2}. \tag{13}$$

Upon substitution of Eqs. (10) and (13) into Eq. (7), α may be approximated as:

$$\begin{aligned}\alpha = \frac{A_G}{A} &\approx \frac{sw\left(1 + \frac{\pi}{4}\right) - \delta(s + w)\left(2 + \frac{\pi}{2}\right) + (4 + \pi)\delta^2}{2} \\ &\approx \frac{1}{2}\left(1 + \frac{\pi}{4}\right) - \delta\frac{(s + w)}{sw}\left(1 + \frac{\pi}{4}\right).\end{aligned} \tag{14}$$

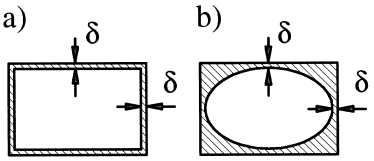

Fig. 11. Schematic representation of two assumed cross-section shapes for a Taylor bubble in the rectangular cross section.

The results of this approximation for the four different non-circular channels are listed in Table 3. For the rectangular channels one can use the distribution parameter listed in Table 2 and the drift velocity listed in Table 3 (e.g. Mishima et al., 1993) in order to calculate the transition from slug to churn flow. Not known a priori is the drift velocity for the rhombic and the equilateral triangular channel. Compared to the rectangular geometry, the width (w_1) and the gap (s_1) for the rhombic geometry are defined as:

$$w_1 = c_1 + c_2 = \frac{b}{2\sin(\varphi)} + \frac{b\cos(2\varphi)}{\sin(\varphi)} = \frac{b}{2\sin(\varphi)}(1 + \cos(2\varphi)),$$

$$s_1 = c_1 \sin(2\varphi) = b\cos(\varphi).$$

The terms c_1 and c_2 are depicted in Fig. 12. For the equilateral triangular geometry we use the same definition as for the circular tube. Both expressions for the drift velocity are shown in Table 3. Figs. 5–8 show the transition criterion (Eq. (9)) from slug to churn flow compared with the experimental results. In this study, we relate the channel length influence (discussed by Jayanti and Hewitt, 1992) to the L/d_h-relation of the visual section where the flow patterns are observed. The only unknown is the constant C, which for flooding should have a value between 0.75 and 1 depending on the outlet condition. Considering the critical gas velocity, Jayanti and Hewitt show that a value of $C = 1.2$ agrees well with the data at low liquid flow rates, however, these value fails for predicting the flooding phenomenon. For the new model of the slug to churn transition (Eq. (9)), which is different to the flooding model (Eq. (4)), Jayanti and Hewitt only postulated that C must have a value near unity. In fact, there is a good agreement between the theoretical prediction and the experimental results presented here with a value of $C \approx 1.2$. The exact values for the constant C used in the figures are shown in Table 4.

3.3. The transition from dispersed bubble to slug flow

In the literature two different models exist basing on the work from Taitel and Dukler (1976) to predict the transition from dispersed bubble to slug flow in vertical two-phase flow. One is a physical model in consideration of the bubble breakup proposed by Barnea et al. (1982) and the other is an empirical correlation developed by Weisman and Kang (1981). The empirical correlation from Weisman and Kang (1981) suggests that the transition is

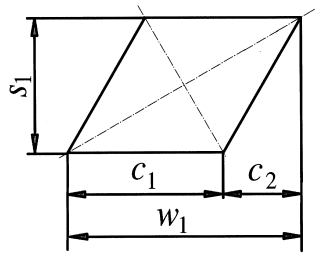

Fig. 12. Presentation of the definition for the width (w_1) and the gap (s_1) using a rhombic cross-section.

independent of the gas flow rate and the transition will occur if

$$\frac{\sqrt{|\frac{dp}{dx}|_{LS}}}{\Delta\rho g} = 1.7\left(\frac{\sigma}{\Delta\rho g d_h^2}\right)^{0.25}, \tag{15}$$

where $|dp/dx|_{LS}$ is the pressure drop per unit length of liquid flowing alone in the tube/channel

$$|\frac{dp}{dx}|_{LS} = \frac{1}{2}\lambda_{LS}\frac{\rho_L U_{LS}^2}{d_h}. \tag{16}$$

Here, λ_{LS} is turbulent friction coefficient obtained from the λ versus Re relationship for turbulent flow:

$$\lambda_{LS} = \frac{C_T}{Re_{LS}^{0.25}} \quad \text{with } Re_{LS} = \frac{\rho_L U_{LS} d_h}{\mu_L} \quad \text{if } Re_{LS} \geq 2100, \tag{17}$$

where μ_L is the dynamic viscosity of the liquid and the proportionality coefficient C_T is called geometry factor for turbulent flow and depends on the geometry factor for laminar flow C_L. The book of Shaw and London (1978) contains C_L-tables for various kinds of channels and an expression for calculating C_T was given by Sadatomi et al. (1982). Additionally, a correction ϕ_1 for the superficial gas velocity and ϕ_2 for the superficial liquid velocity has been applied to the transition line to predict the transition for all mentioned fluid properties and pipe diameters:

$$\phi_1 = 1$$

$$\phi_2 = \left(\frac{\rho_L}{\rho_{sL}}\right)^{-0.33}\left(\frac{d_h}{d_{s1}}\right)^{0.16}\left(\frac{\mu_{sL}}{\mu_L}\right)^{0.09}\left(\frac{\sigma}{\sigma_s}\right)^{0.24}, \tag{18}$$

with $d_{s1} = 25.4$ mm, $\rho_{sL} = 1000$ kg/m^3, $\mu_{sL} = 10^{-4}$ Ns/m^2 and $\sigma_s = 0.07$ N/m. This model shows agreement for the transition from dispersed bubble to slug flow for large diameter tubes. However, since the model has only a small diameter influence the prediction fails for small diameter tubes.

The model from Barnea et al. (1982) is based on the concept that the turbulent forces for the dispersed bubble flow regime do overcome the surface tension forces of the gas bubbles to disperse the gas into small bubbles. In the dispersed bubble flow regime the bubbles are

Table 4
Values of the constant C for the different cross-sections

	Circular	Rectangular	Rectangular	Rhombic	Equilateral triangular
		$(s/w = 0.97)$	$(s/w = 0.7)$		
C_{exp}	1.21	1.18	1.17	1.19	1.20

spherical, and thus small enough to prevent agglomeration and coalescence. Barnea et al. (1982) suggest the following relation for the stable dispersed bubble diameter:

$$d_{\max} = \left(0.725 + 4.15\sqrt{\frac{U_{GS}}{U_M}}\right)\left(\frac{\rho_L}{\sigma}\right)^{3/5}\left(\frac{2f_M}{d_h}U_M^3\right)^{-2/5}, \tag{19}$$

where $U_M(= U_{GS} + U_{LS})$ is the mixture superficial velocity and f_M is the friction factor for the mixture velocity defined as:

$$f_M = \frac{0.046}{Re_M^{0.2}} \quad \text{with } Re_M = \frac{\rho_L U_M d_h}{\mu_L} \quad \text{if } Re_M \geq 2100. \tag{20}$$

When the bubble size increases, the bubbles are distorted from the spherical shape and coalescence sets in. The critical bubble size is defined for a bubble rising at constant velocity:

$$d_{crit} = 2\sqrt{\frac{0.4\sigma}{\Delta\rho g}}, \tag{21}$$

and the transition occurs when $d_{\max} > d_{crit}$. This model shows also agreement for the transition from dispersed bubble to slug flow for large diameter tubes. If the tube diameter is larger than the one used in this investigation or e.g. Lowry and Kawaji (1988) and Fukano and Kariyasaki (1993), one could conclude that the transition is in the same region. Fig. 4 shows the results for the transition models from Weisman and Kang (1981) and Barnea et al. (1982) compared to the experimental results for the circular tube, whereas the superficial liquid velocity for the model from Weisman and Kang (1981) is shown as U_{LS}/ϕ_2. From the figure, it is clearly seen that both models fail to predict the transition accurately.

In the following, we improve the empirical correlation from Weisman and Kang (1981) (Eq. (15)) with a hyperbolic formula in order to show that the transition from dispersed bubble to slug flow also depends on the superficial gas velocity for small diameter tubes/channels. The new correlation for the circular tube has been worked out as follows:

$$\sqrt{\frac{|\frac{dp}{dx}|_{LS}}{\Delta\rho g}} = 1.7\left(\frac{\sigma}{\Delta\rho g d_h^2}\right)^{0.25}\left(\frac{0.65U_{GS}}{C_0^3 V_{GU} + U_{GS}}\right)^{7/8}, \tag{22}$$

where the distribution parameter is listed in Table 2 and V_{GU} for slug flow as shown in Table 3 serves as a characteristic drift velocity for the transition. The good agreement between the improved empirical correlation (Eq. (22)) displayed as U_{LS}/ϕ_2 and the experimental results for the circular tube is shown in Fig. 4.

For tube diameters different from the one used here the correction factor ϕ_2 is extended with the following correlation:

$$\phi_{2,new} = \phi_2\left(\frac{d_{s2}}{d_h}\right)^{0.33}, \tag{23}$$

with $d_{s2} = 5.9$ mm. In Fig. 13, we compare the models from Weisman and Kang (1981), Barnea et al. (1982) and the improved empirical correlation (Eq. (22)) for three different tube diameters, where the model from Weisman and Kang is shown as U_{LS}/ϕ_2 and Eq. (22) is shown as $U_{LS}/\phi_{2,new}$. From the figure, it is clearly seen that the model from Weisman and Kang has only a small diameter influence and the model from Barnea et al. has only a small superficial gas velocity influence in contrast to the improved correlation. In Figs. 14–18, the improved correlation and the model published by Barnea et al. (1982) are compared with experimental data: in Figs. 14 and 15 for an air–water system in a 25.4 and 50.8 mm diameter circular tube according to Shoham (1982), in Figs. 16 and 17 for an air–water system in a 4.0 and 12.3 mm diameter circular tube according to Barnea et al. (1983) and in Fig. 18 for an air–water system in a 2.4 mm diameter circular tube according to Fukano and Kariyasaki (1993). The proposed model gives a good prediction for the transition from dispersed bubble to slug flow in the overall range of pipe diameter from 2.4 to 50.8 mm. The predictions are good with respect to both the basic trends of the transition and also to their absolute location.

To predict the transition from dispersed bubble to slug flow for a non-circular channel, the use of the new correlation (22) is satisfactory in consideration of the distribution parameters listed in Table 2 and the drift velocities listed in Table 3. For the correction factor we found additional dependencies:

$$\phi_{2,\text{non-circular}} = \phi_{2,\text{new}} \left(\frac{A}{\frac{\pi}{4} d_h^2} \right) \left(\frac{L_{C1}}{L_{C2}} \right)^{0.33}, \tag{24}$$

where the first term compares the cross-section area of the non-circular channel with an equivalent cross-section area of a circular tube. The second term displays the dependency of two characteristic length of the channel geometry L_{C1} and L_{C2} on the transition. For a rectangular channel we use the gap of the channel for $L_{C1} = s$ and the width of the channel for $L_{C2} = w$ and for the rhombic channel the characteristic length are the height $L_{C1} = h$ and the breadth $L_{C2} = w$ of the channel. For the equilateral triangular channel the characteristic length are for L_{C1} the perimeter of the triangular and for L_{C2} the perimeter of the incircle. The results are shown in Figs. 5–8, whereas the transition from dispersed bubble to slug flow is shown as $U_{LS}/\phi_{2,\text{non-circular}}$.

3.4. Overall flow maps

The correlations proposed in Sections 3.1–3.3 could be used to construct an overall flow pattern map for given channel dimensions and for a given fluid system with attention to the hydraulic diameter. Only the transition to annular flow is not modeled. For predicting this transition one can use the transition model published by Wilmarth and Ishii (1994) for small diameter tubes and the theoretical models from Barnea et al. (1982), Mishima and Ishii (1984) or McQuillan and Whalley (1985) for larger tubes. In Fig. 19 the transition lines are plotted for all channel geometries used in this investigation. Care should be taken only on the theoretical prediction for the transition from one flow regime to another flow regime. The transitions have been correlated for a definite transition point/line. It should be noted that the

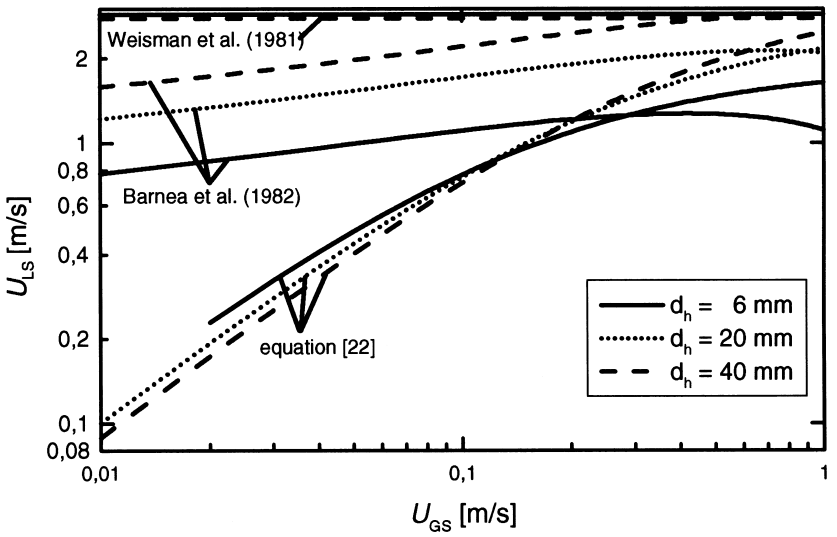

Fig. 13. Comparison of the model from Weisman and Kang (1981), Barnea et al. (1982) and the improved empirical correlation (Eq. (22)) for the transition from dispersed bubble to slug flow for three different tube diameters.

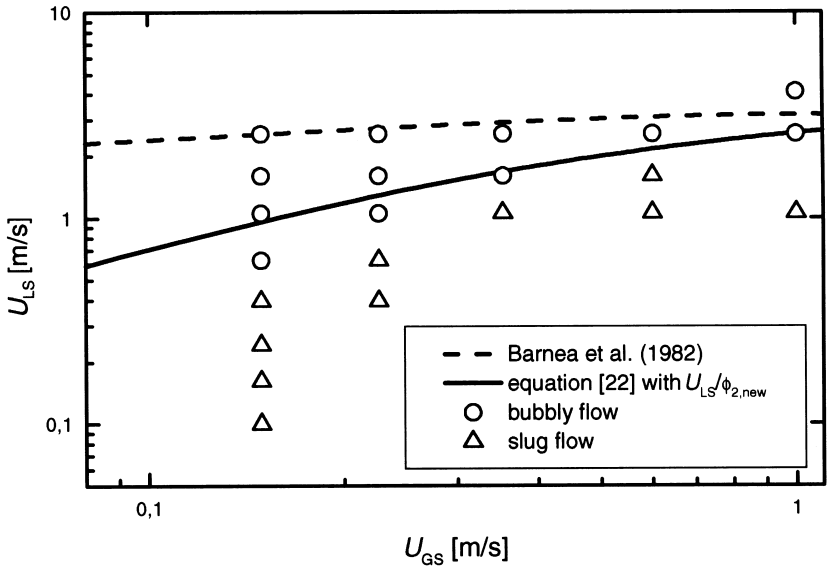

Fig. 14. Comparison of Eq. (22) and the model published by Barnea et al. (1982) with data from Shoham (1982) (air–water, 25°C, $d_h = 50.8$ mm) for the transition from dispersed bubble to slug flow.

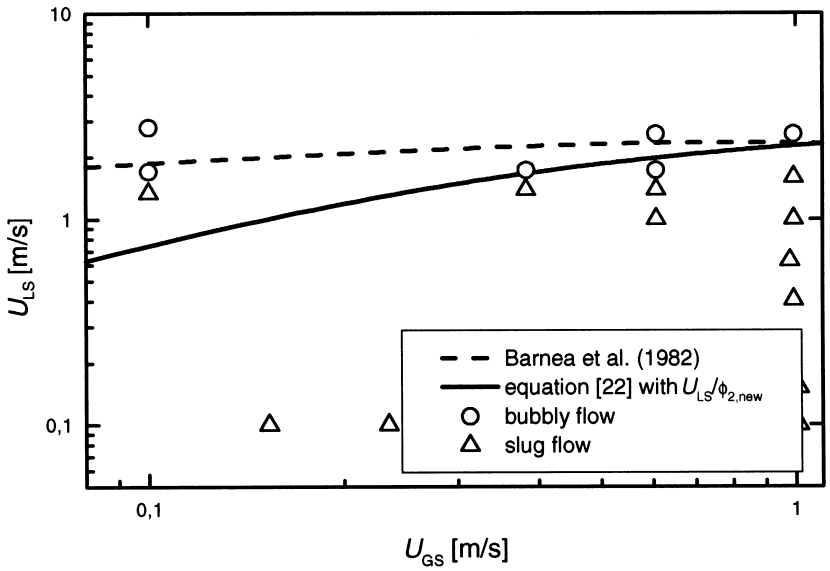

Fig. 15. Comparison of Eq. (22) and the model published by Barnea et al. (1982) with Shoham (1982) data (air–water, 25°C, $d_h = 25.4$ mm) for the transition from dispersed bubble to slug flow.

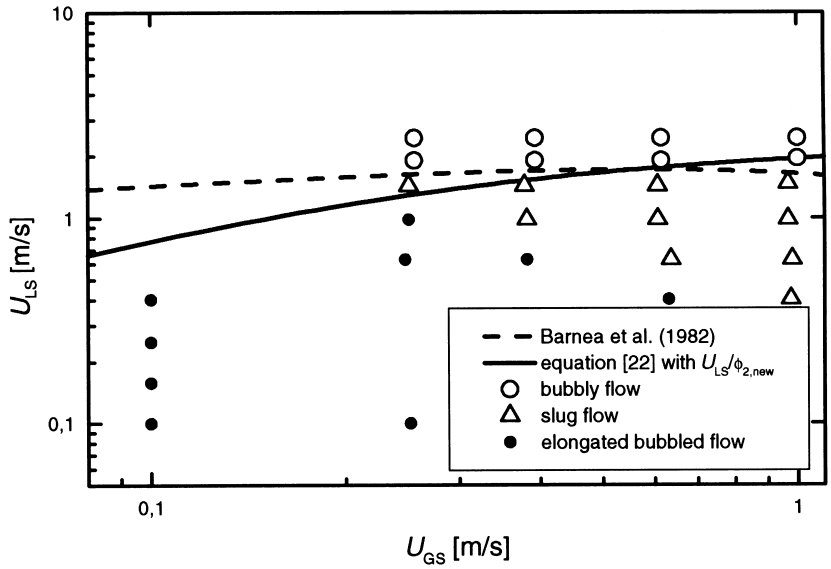

Fig. 16. Comparison of Eq. (22) and the model published by Barnea et al. (1982) with data from Barnea et al. (1983) (air–water, 25°C, $d_h = 12.3$ mm) for the transition from dispersed bubble to slug flow.

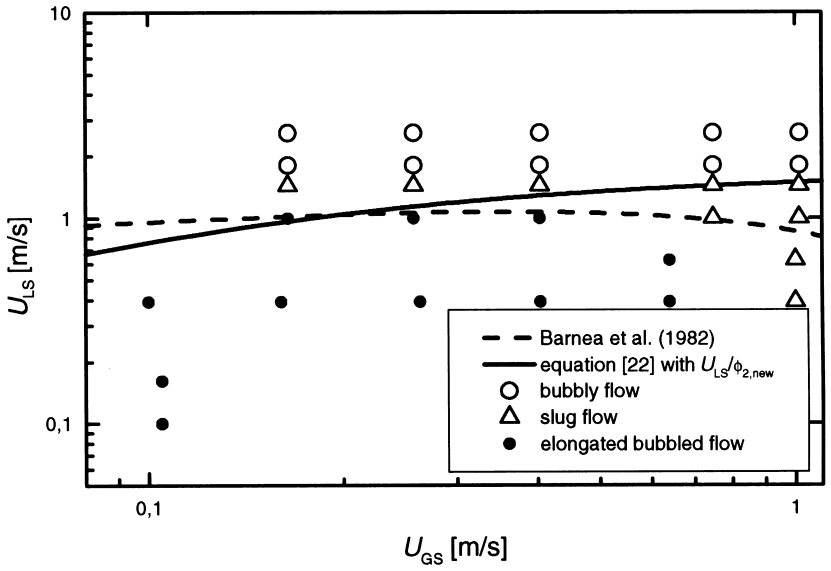

Fig. 17. Comparison of Eq. (22) and the model published by Barnea et al. (1982) with data from Barnea et al. (1983) (air–water, 25°C, $d_h = 4.0$ mm) for the transition from dispersed bubble to slug flow.

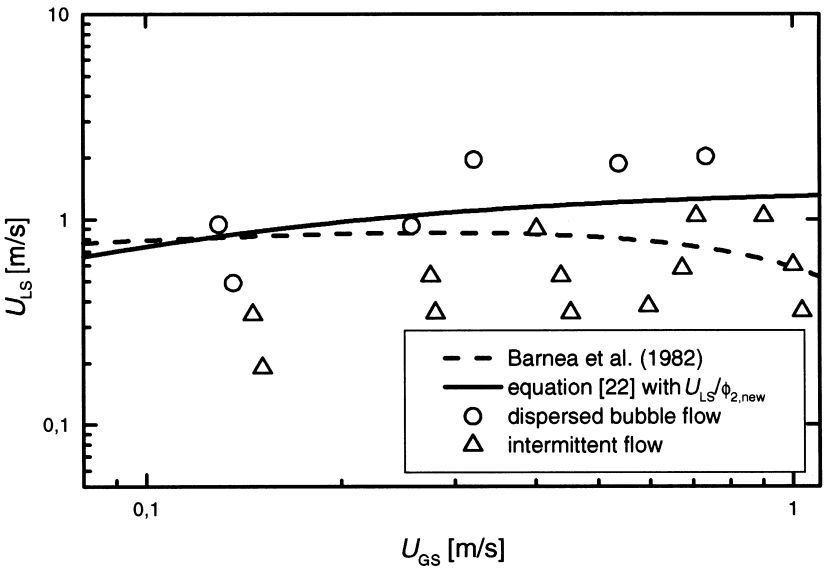

Fig. 18. Comparison of Eq. (22) and the model published by Barnea et al. (1982) with data from Fukano and Kariyasaki (1993) (air–water, $d_h = 2.4$ mm) for the transition from dispersed bubble to intermittent flow.

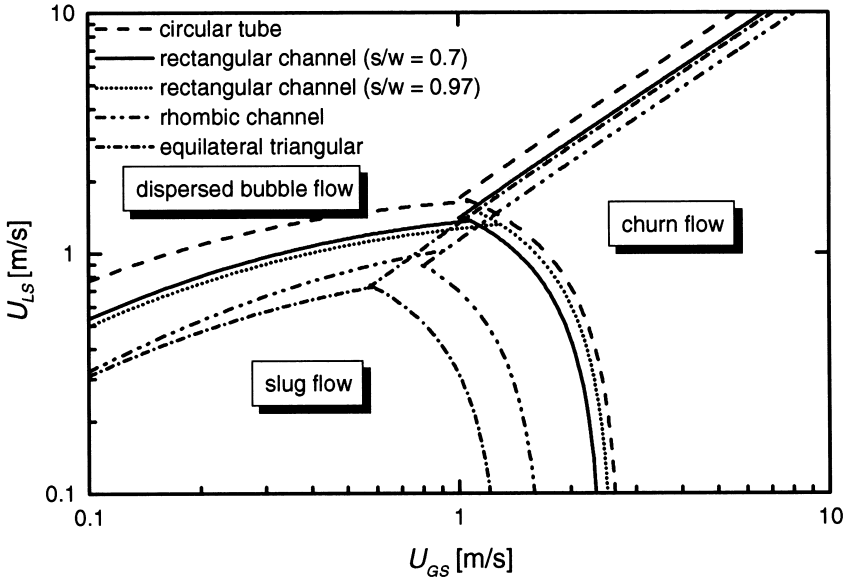

Fig. 19. Overall flow map for all cross-sections examined in this investigation.

transition is a gradual phenomenon and consequently the transition could not be modeled with a 'single small curve'. Nevertheless, the theoretical models give a good prediction for the transition region.

From Fig. 19 it may be seen, that an influence of the channel geometry on the flow pattern transition does exist. The influence from the channel geometry results from the steeper radial distribution of the phases and/or velocities and from the turbulent secondary flow which occurs in non-circular channels. For the transition from dispersed bubble to churn flow the higher radial distribution together with the turbulent secondary flow prevents the agglomeration of the gas bubbles and the turbulent secondary flow causes an additional shear force acting on the small gas bubbles. A similar influence occurs on the transition from dispersed bubble to slug flow. For the transition from slug to churn flow the turbulent secondary flow influences the effect of breakup of the Taylor bubble and the transition occurs at a lower superficial gas velocity compared to the circular tube.

4. Concluding remarks

Experimental results for air-water two-phase flow in one circular tube and four different non-circular channels (with rectangular, rhombic and equilateral triangular cross-section) were carried out. The hydraulic diameter ($d_h \approx 6$ mm) lies in the typically range used for plate-fin heat exchangers. A comparison of the results for the different cross-sections emphasizes the influence of the superficial liquid and gas velocity as well as the influence of the channel geometry on the transition between two different flow patterns. The transition from dispersed

bubble to churn flow occurs at higher superficial gas velocities, the transition from dispersed bubble to slug flow at lower superficial liquid velocities and the transition from slug to churn flow at lower superficial gas velocities compared to the circular tube. The main reason for this shifting of the transition regions does result from the turbulent secondary flow that occurs in non-circular channels and from the steeper radial distribution of the phases and/or velocities.

The experimental results were compared with improvements of existing models for the transition between two different flow patterns. The results reveal good abilities of the drift flux model to predict the transition from dispersed bubble to churn flow with $\alpha = 0.30$ for small tube/channel diameters. For the rhombic and equilateral triangular channel new distribution parameters have been determined, which serve as excellent parameters. For the transition from dispersed bubble to slug flow, an empirical correlation depending on the superficial liquid and gas velocity is suggested which shows good agreement with the experiments. A correction factor was formulated to adopt the empirical correlation for non-circular channels as well as for large tube diameters. Concerning the transition from slug to churn flow, it was found, that the flooding model predicts the transition for circular tubes and also for non-circular channels. Thus, the superficial Taylor bubble velocity was calculated with the drift flux model and the void fraction was approximated with a geometrical analysis. For the rhombic channel, a new relation for the drift velocity for slug flow is determined depending on the channel dimensions. For the unknown constant C a value of 1.2 serves well.

Acknowledgements

The work was supported by the German Space Agency (DLR) under grand FKZ 50WM9443. The authors wish to express their gratitude to H. Faust and F. Ciecior for the preparation of the experiment facility and to L. Nowag for the performance of the experiments.

References

Barnea, D., Shoham, O., Taitel, Y., 1982. Flow pattern transition for vertical downward two phase flow. Chem. Engng Sci 37, 741–746.

Barnea, D., Luninski, Y., Taitel, Y., 1983. Flow pattern in horizontal and vertical two phase flow in small diameter pipes. Can. J. Chem. Engng 61, 617–620.

Bell, K.J., 1988. Two-phase flow regime consideration in condenser and vapor design. Int. Commun. Heat Mass Transfer 15, 429–448.

Brotz, W., 1954. Über die Vorausberechnung der Absorptionsgeschwindigkeit von Gasen in strömenden Flüssigkeiten. Chem. Engng Sci 41, 159–163.

Duns Jr, H., Ros, N.C.J., 1963. Vertical flow of gas and liquid mixtures from boreholes. In: Proc. 6th World Petroleum Congress, Frankfurt.

Fukano, T., Kariyasaki, A., 1993. Characteristics of gas–liquid two-phase flow in a capillary tube. Nucl. Engng Design 141, 59–68.

Hewitt, G.F., Hall-Taylor, N.S., 1970. Annular Two-Phase Flow. Pergamon Press, New York.

Hewitt, G.F., Wallis, G.B., 1963. Flooding and associated phenomena in falling film flow in a vertical tube. UKAEA Report No. AERE R4022.

Jayanti, S., Hewitt, G.F., 1992. Prediction of the slug-to-churn flow transition in vertical two-phase flow. Int. J. Multiphase Flow 18, 847–860.

Jones, O.C., Zuber, N. 1979. Slug-annular transition with particular reference to narrow rectangular ducts. Two-Phase Momentum. In: Heat and Mass Transfer in Chemical, Process, and Energy Engineering Systems. Hemispere, Washington, pp. 345–355.

Liu, T.J., 1993. Bubble size and entrance length effects on void development in a vertical channel. Int. J. Multiphase Flow 19, 99–113.

Lowry, B., Kawaji, M., 1988. Adiabatic vertical two-phase flow in narrow flow channels. AIChE Symp. Series 84, 133–139.

McQuillan, K.W., Whalley, P.B., 1985. Flow patterns in vertical two-phase flow. Int. J. Multiphase Flow 11, 161–175.

Mishima, K., Hibiki, T., 1996. Some characteristics of air-water two-phase flow in small diameter vertical tubes. Int. J. Multiphase Flow 22, 703–712.

Mishima, K., Hibiki, T., Nishihara, H., 1993. Some characteristics of gas–liquid flow in narrow rectangular ducts. Int. J. Multiphase Flow 19, 115–124.

Mishima, K., Ishii, M., 1984. Flow regime transition criteria for upward two-phase flow in vertical tubes. Int. J. Heat Mass Transfer 27, 723–737.

Nicklin, D.J., Wilkes, J.O., Davidson, J.F., 1962. Two-phase flow in vertical tubes. Trans. J. Chem. Engng 40, 61–68.

Nikuradse, J., 1933. Strömungsgesetze in rauhen Rohren. VDI Forschungsheft 361, Forschungsheft 361, English Trans., NACA Tech. Mem., 1292.

Owen, D.G., 1986. An empirical and theoretical analysis of equilibrium annular flow. Ph.D. Thesis, University of Birmingham, UK.

Radovcich, N.A., Moises, R., 1962. The transition from two phase bubble to slug flow. MIT Report 7-7673-22.

Sadatomi, Y., Sato, T., Saruwatari, S., 1982. Two-phase flow in vertical noncircular channels. Int. J. Multiphase Flow 8, 641–655.

Shaw, R.K., London, A.L., 1978. Laminar Flow Forced Convection in Ducts. Academic Press, New York.

Shoham, O., 1982. Flow pattern transition and characterization in gas–liquid two phase flow in inclined pipes. Ph.D. Thesis, Tel-Aviv University, Ramat-Aviv, Israel.

Taitel, Y., Barnea, D., Dukler, A.E., 1980. Modeling flow pattern transition for steady upward gas-liquid flow in vertical tubes. AIChE J 26, 345–354.

Taitel, Y., Dukler, A.E., 1976. A model for predicting flow regime transitions in horizontal and near horizontal flow. AIChE J 22, 47–55.

Wallis, G.B., 1961. Flooding velocities for air and water in vertical tubes. UKAEA Report No. AEEW-R123.

Wallis, G.B., 1969. One-Dimensional Two-Phase Flow. McGraw-Hill, New York.

Weisman, J., Kang, S.Y., 1981. Flow pattern transition in vertical and upwardly inclined lines. Int. J. Multiphase Flow 7, 271–291.

White, F.M., 1986. Fluids Mechanics, 2nd ed. McGraw-Hill, New York.

Wilmarth, T., Ishii, M., 1994. Two-phase flow regimes in narrow rectangular vertical and horizontal channels. Int. J. Heat Mass Transfer 37, 1749–1758.